Impact of Irradiation Side on Neutron-Induced Single-Event Upsets in 65-nm Bulk SRAMs

Shinichiro Abe, Wang Liao, Seiya Manabe, Tatsuhiko Sato, Masanori Hashimoto, and Yukinobu Watanabe

***Abstract*— The impact of the irradiation side on the cross sections of single-event upsets (SEUs) induced by neutrons was investigated by performing neutron irradiation measurements and simulations. A test board equipped with 65-nm bulk 6-T CMOS static random access memories was irradiated by quasi-monoenergetic neutrons, and the number of SEUs was counted. The number of SEUs obtained by the board-side irradiation was approximately 20% to 30% smaller than that obtained by irradiation on the plastic package side. We also investigated the impact of irradiation side on the soft error rates (SERs) obtained with by the terrestrial neutron energy spectrum via a Monte Carlo simulation. The SER obtained from the plastic package side irradiation was approximately twice that obtained for the board side irradiation, indicating that SERs can be reduced by equipping the device with the package side facing downward. Additionally, based on the simulation, the atomic composition of the material placed in front of the memory chip has a considerable influence on the SER because production yields and angular distributions of secondary H and He ions (the main causes of SEUs) depend on the composition. In particular, the existence of hydrides, such as plastic, considerably increases the SER because of the higher production yields of secondary H ions that are generated via elastic scattering of neutrons with hydrogen atoms.**

***Index Terms*— Monte Carlo simulation, neutrons, PHITS, single-event upset (SEU), soft errors.**

I. Introduction

SINGLE-EVENT upsets (SEUs) caused by secondary cosmic-ray neurons have been recognized as a serious reliability problem for microelectronic devices on the ground level. Validation of soft error rates (SERs) is necessary to assure the reliability of devices. Field tests [1] provide the most realistic SERs; however, they require a huge number of devices and a very long measurement time. Acceleration tests at neutron facilities [2]–[5] provide SERs more quickly than field tests; however, some corrections are required to derive realistic SERs in the actual environment or to compare them with other measured data. Therefore, it should be determined how much various conditions affect the measurements.

In our previous study [6], [7], we performed simulations of neutron-induced soft errors in MOSFETs with 65- to 25-nm bulk CMOS technologies using a multiscale Monte Carlo simulation code system PHYSERD. We found that secondary light charged particles (i.e., H and He ions) generated by nuclear reaction are the main cause of SEUs induced by secondary cosmic-ray neurons because their mean flight path lengths are longer than those for heavy ions. We also performed a simplified simulation to discuss the sufficient size of the reaction volume [7]. We considered only silicon as a reaction volume in that study, whereas transistors placed on a silicon substrate are covered by packaging material, such as plastic. In general, secondary ions are emitted in a forward direction particularly for high-energy emission, and the amount of secondary ions depends on the target materials. Therefore, it is predicted that SERs measured by acceleration tests depend on whether the test board is irradiated by neutrons from the package side or from the board side.

In this paper, we conducted quasi-monoenergetic neutron irradiations from the package side and from the board side of the test board and counted the number of SEUs. We also derived SEU cross sections for a 65-nm bulk static random access memories (SRAM) using a Monte Carlo simulation with monoenergetic neutrons.

II. Experimental Setup

Quasi-monoenergetic neutron irradiation tests were conducted at the Cyclotron and Radioisotope Center (CYRIC) at Tohoku University [8]. Fig. 1 shows the irradiated neutron spectra produced by using the ^{7}Li(p,n)^{7}Be reaction with proton energies of 70 and 30 MeV, where the peak energies of the neutron, E_{peak}, are approximately 65 and 23 MeV, respectively. Fig. 2 shows an image of the tested board that was tested in previous measurements [9], [10]. In total, 16 chips of 65-nm bulk 6-T SRAMs were embedded in the test board that had a thickness of 1.6 mm and were sealed by plastic. Each chip contains 12-Mbit memories. The 6-T cell layout was designed for a commercial product.

Static tests with a hold time of 300 s were performed using the same method as for the previous measurement [9]. The test board was irradiated with neutrons from the package side and from the board side as shown in Fig. 2(a) and (b), respectively, and the number of upsets was counted. Measurements were

Manuscript received January 9, 2019; accepted February 25, 2019. Date of publication February 28, 2019; date of current version July 16, 2019. This work was supported by the Japan Science and Technology Agency through the Program on Open Innovation Platform with Enterprises, Research Institute, and Academia.

S. Abe and T. Sato are with Japan Atomic Energy Agency, Ibaraki 319-1195, Japan (e-mail: abe.shinichiro@jaea.go.jp).

W. Liao and M. Hashimoto are with the Department of Information System Engineering, Osaka University, Osaka 565-0871, Japan.

S. Manabe and Y. Watanabe are with the Department of Advanced Energy Engineering Science, Kyushu University, Fukuoka 816-8580, Japan.

Color versions of one or more of the figures in this paper are available online at http://ieeexplore.ieee.org.

Digital Object Identifier 10.1109/TNS.2019.2902176

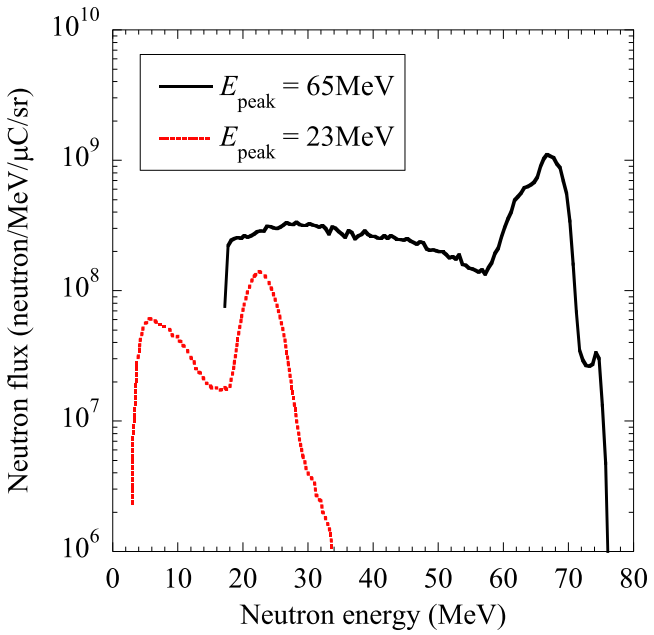

Fig. 1. Energy spectra of quasi-monoenergetic neutron beam at CYRIC.

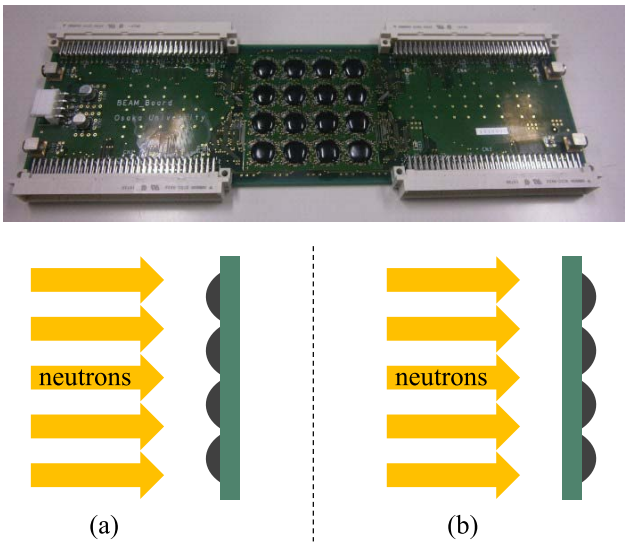

Fig. 2. Image of device board under test [8], [9] and schematic of the irradiation direction. (a) Package-side irradiation. (b) Board-side irradiation.

performed with operation voltages of 0.5, 0.9, and 1.2 V. Approximately 20 memory cells or fewer could not hold their stored values at an operation voltage of 0.5 V, while a nonworkable memory cell did not exist with an operation voltage of 1.2 V. These nonworkable memory cells were excluded before the neutron irradiations. The number of nonworkable memory cells did not increase during the radiation test.

III. Simulation Method

For the Monte Carlo simulation, PHITS ver. 3.07 [11] was applied to simulate radiation transport and nuclear reaction. Neutron reactions below 20 MeV were calculated by the event generator mode (e-mode) ver. 2 [12], [13] with JENDL-4.0 [14], and those above 20 MeV were calculated by the intranuclear cascade of Liege [15] model and the generalized evaporation model (GEM) [16]. The collected charge was

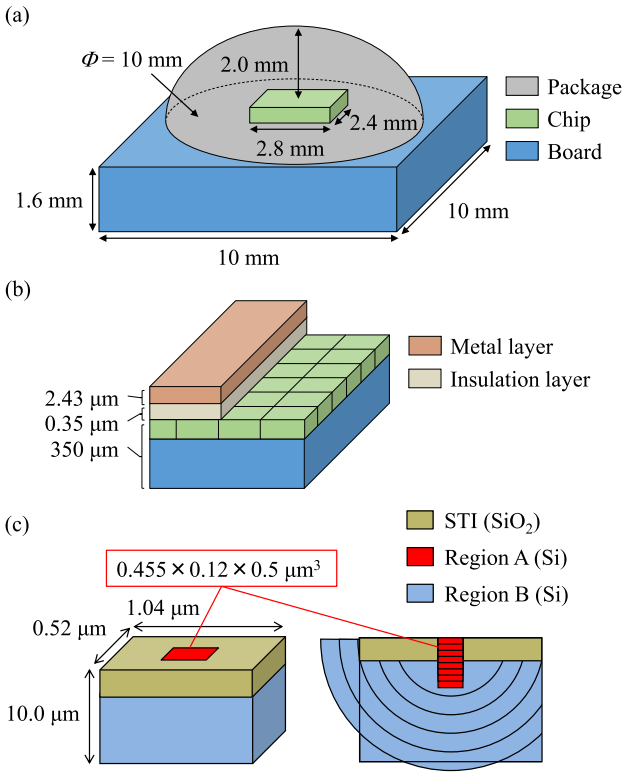

Fig. 3. Simulation structure of (a) test board, (b) chip, and (c) analysis volume for MSV model.

estimated from the energy deposition using the multiple sensitive volume (MSV) model [17]. To define the size and charge collection efficiency (CCE), the charge collection process in a 65-nm bulk NMOSFET was investigated systematically by a 3-D TCAD simulator, HyENEXSS [18]–[20]. The same parameter set for the NMOSFET used in the previous study [21] was adopted for the device simulation. The width of the active area was adjusted to reproduce the NMOSFET in the SRAM cell used for the experimental measurement.

The configuration of the test target used in the simulation is shown in Fig. 3. A chip covered with plastic ($C_{18}H_{19}O_5$) was placed on a 10 mm × 10 mm × 1.6 mm board. In the chip, 12-Mbit SRAM cells were placed as a 2-D grid. A 0.35-μm-thick silicon dioxide insulation layer was on top of the SRAM cells, and a 2.43-μm-thick metal layer made of copper and silicon dioxide was on top of the insulation layer. Fig. 3 also shows the configuration of the analysis volume for the MSV model. The analysis volume was divided into region A and region B. Region A was defined by the active area of the NMOSFET and had an effective funneling length of 0.5 μm, and region B was defined as the remainder of the NMOSFET. The collected charge was estimated when a charged particle struck region A because they are expected to collect charges because of funneling and be primarily responsible for SEUs. To keep the difference in the CCEs of the two adjacent sensitive volumes (SVs) below 10 %, region A was subdivided into 142 SVs, and region B was subdivided into 31 SVs. Figs. 4 and 5 show the CCEs for the 65-nm bulk NMOSFET with an operation voltage of 1.2 V as calculated by HyENEXSS. The CCEs are plotted as a function of the

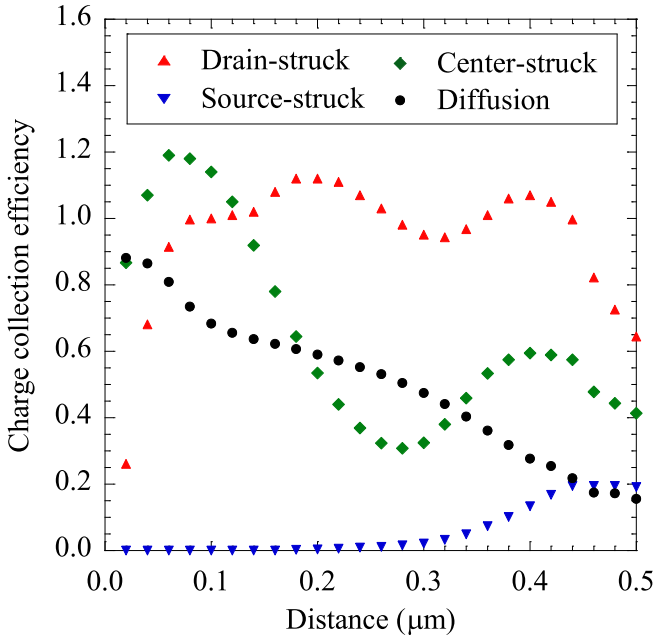

Fig. 4. CCE in region A calculated by HyENEXSS.

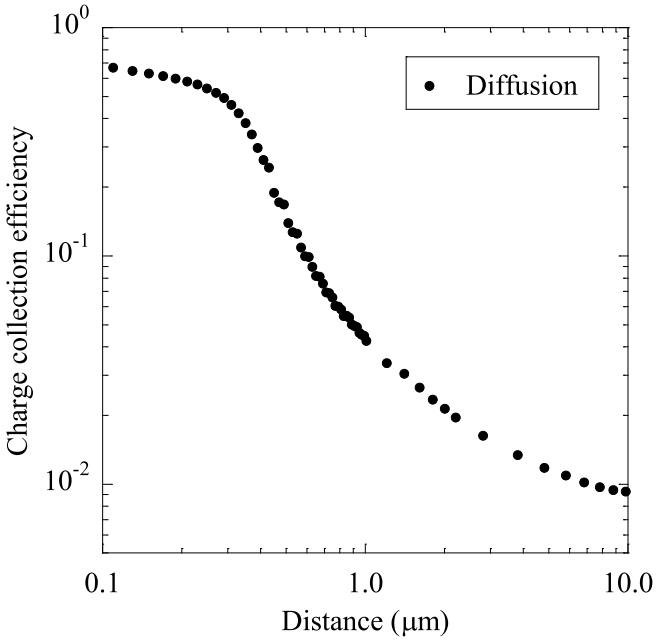

Fig. 5. CCE in region B calculated by HyENEXSS.

distance between each SV and the center of the transistor surface. The CCEs in region A were switched event-by-event depending on whether ions strike in the depletion regions because they depend on the ion struck position. When ions struck both depletion regions, the CCE obtained by the center strike was applied.

The collected charge, Q_{collect}, is approximated in the MSV model using the following equation:

$$Q_{\text{collect}} = \frac{e}{E_{\text{pair}}} \sum \alpha_i \times E_{\text{dep},i} \tag{1}$$

where α_i is the CCE of the ith SV, $E_{\text{dep},i}$ is the energy deposited in the ith SV, e is the elementary charge, and E_{pair} is the average energy required to generate an electron–hole pair (3.6 eV in silicon).

In this paper, we investigated plastic and alumina as the package materials. Neutron irradiations of the test target were simulated, and the number of events, $N(E_{\text{n}}, q)dq$, with the collected charge in $[q, q + dq]$ at the incident neutron energy, E_n, was derived. The SEU cross section is calculated as a function of the critical charge, Q_{crit}, as follows:

$$\sigma_{\text{SEU}}(E_n, Q_{\text{crit}}) = \frac{A}{N_{\text{in}} \times N_{\text{bit}}} \int_{Q_{\text{crit}}}^{\infty} N(E_n, q)dq \tag{2}$$

where A is the surface area of the test target shown in Fig. 3 (i.e., $A = 1.0$ cm^2), N_{in} is the number of incident neutrons in the PHITS calculation, and N_{bit} is the number of SRAM cells placed in the test target. In this paper, we show the result for $Q_{\text{crit}} = 0.28$ and 1.0 fC to investigate how the variation in Q_{crit} affects the SEU cross sections. The SER is calculated via the following equation:

$$\text{SER} = \int \phi(E)\sigma_{\text{SEU}}(E)dE \tag{3}$$

where $\phi(E)$ is the neutron flux.

In addition to simulations of monoenergetic neutron irradiations on the test target, we also performed simulations of quasi-monoenergetic neutron irradiations on the test target to consider the fine structure of the neutron spectrum.

IV. Results and Discussion

A. Comparison Between Experiment and Simulation

Fig. 6(a) and (b) show the measured number of SEUs obtained by irradiations of quasi-monoenergetic neutrons with the peak energies of 65 and 23 MeV from the package side and from the board side. The number of SEUs was normalized by the measured result obtained for the board side irradiation with an operation voltage of 1.2 V. The number of measured SEUs for the board-side irradiation was approximately 20% to 30% smaller than those for the package-side irradiation regardless of the operation voltage.

Fig. 7 shows the ratio of the number of SEUs obtained in the simulation to that obtained in the experiment for each irradiation test at an operation voltage of 1.2 V. The range of expected critical charge is also shown in Fig. 7. In this range, the number of SEUs obtained via the simulation is the same as that obtained from the experiment; however, the simulation underestimates the measurement result obtained via irradiation with quasi-monoenergetic neutrons with the peak energy of 23 MeV from the board side. The cause of the underestimation will be discussed later. In the case of the simulation, the number of SEUs for the board-side irradiation was approximately 30% to 50% less than that for the package side irradiation.

B. Energy Dependence of SEU Cross Sections

Fig. 8 shows the simulation results of monoenergetic neutron-induced SEU cross sections for the 65-nm bulk CMOS SRAM plotted as a function of incident neutron energy. The SEU cross sections for the board-side irradiation and the

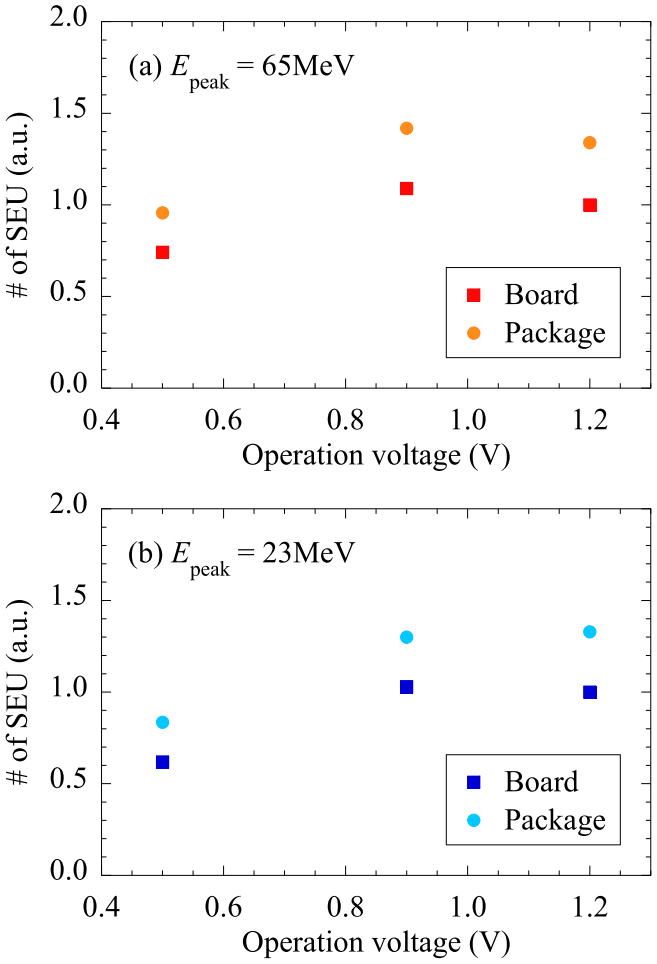

Fig. 6. Measured number of SEUs obtained by irradiations of quasi-monoenergetic neutrons with the peak energies of (a) 65 MeV and (b) 23 MeV.

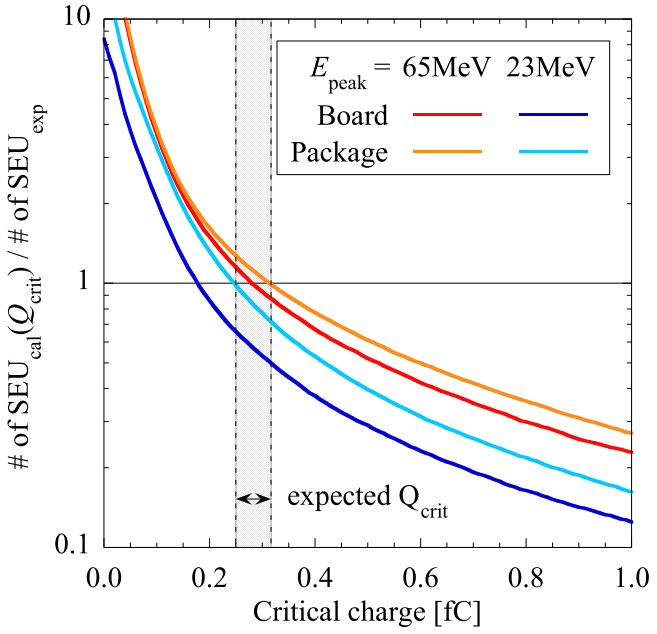

Fig. 7. Ratio of the number of SEUs obtained in the simulation to that obtained in the experiment for each irradiation test with at an operation voltage of 1.2 V.

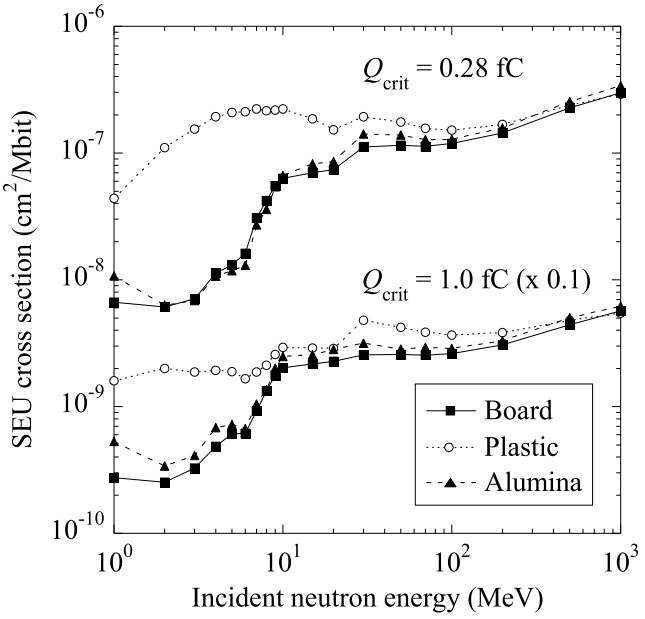

Fig. 8. Monoenergetic neutron-induced SEU cross sections for $Q_{crit} = 0.28$ and 1.0 fC calculated by PHITS + MSV model.

alumina package-side irradiation sharply decrease at approximately several megaelectronvolts. In the previous study [7], the sharp decrease in SEU cross section occurred due to the threshold energies of Si(n, p) and Si(n, α) reactions because secondary H and He ions were the main cause of the SEUs. The threshold energies of the Al(n, p), Al(n, α), O(n, p), and O(n, α) reactions are also several MeV. However, the SEU cross sections for the plastic package side irradiation did not considerably change at approximately several megaelectronvolts. In addition, the SEU cross sections for the plastic package-side irradiation increased slightly at approximately several tens of mega electronvolts, whereas those for the board-side and alumina package-side irradiations decreased as the neutron energy decreased. As a result, the calculated SEU cross sections for the plastic package-side irradiation were larger than those for the board-side and the alumina package-side irradiations, particularly for $Q_{crit} = 0.28$ fC below 20 MeV.

SERs in a terrestrial environment were calculated to discuss how the difference in SEU cross sections affects the SER. In this paper, PHITS-based analytical radiation model in the atmosphere (PARMA) model ver. 4.0 [22], [23] was used to calculate $\phi(E)$. Table I shows the SERs for each condition. The SERs calculated for the plastic package side irradiation were 1.92 and 1.60 times larger than those for the board side irradiation with $Q_{crit} = 0.28$ and 1.0 fC, respectively.

To investigate which secondary ions affect the difference in SEU cross section, the contribution of each secondary ion to the SEU was decomposed, as shown in Figs. 9 and 10. For all irradiations, H and He ions are the main cause of SEUs except for the board and the alumina package irradiation with the neutron energy below 7 MeV. Clearly, the difference in the SEU cross sections is due to secondary H and He ions. Typically, the contribution of H ions for the plastic package-side irradiation is much larger than that for the others for neutron energies below 20 MeV.

TABLE I
ESTIMATED SERS FROM SEU CROSS SECTION AND SECONDARY COSMIC-RAY NEUTRON FLUX [21], [22] FOR EACH CONDITION

SER (FIT/Mbit)	Board side	Plastic side	Alumina side
Q_{crit} = 0.28 (fC)	987.0	1894	1102
Q_{crit} = 1.0 (fC)	227.2	364.7	258.8

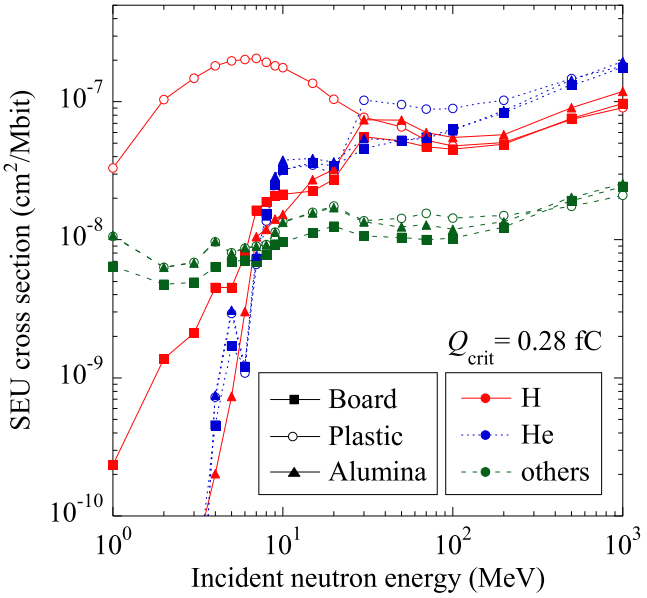

Fig. 9. Contribution of each secondary ion to the SEU cross section for Q_{crit} = 0.28 fC. Lines are for eye guide.

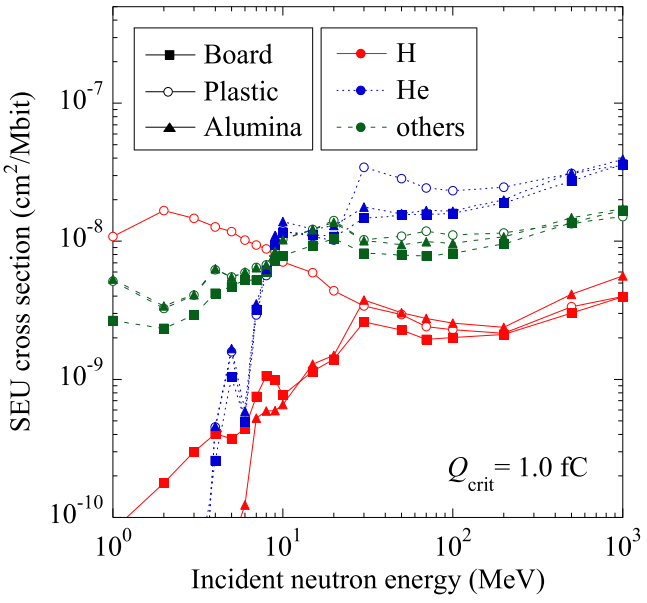

Fig. 10. Contribution of each secondary ion to the SEU cross section for Q_{crit} = 1.0 fC. Lines are for eye guide.

C. Production of Secondary Ions

To investigate the cause of the difference in the contribution of H and He ions to the SEU cross section in detail, mono-energetic neutron irradiations on silicon, plastic, and alumina

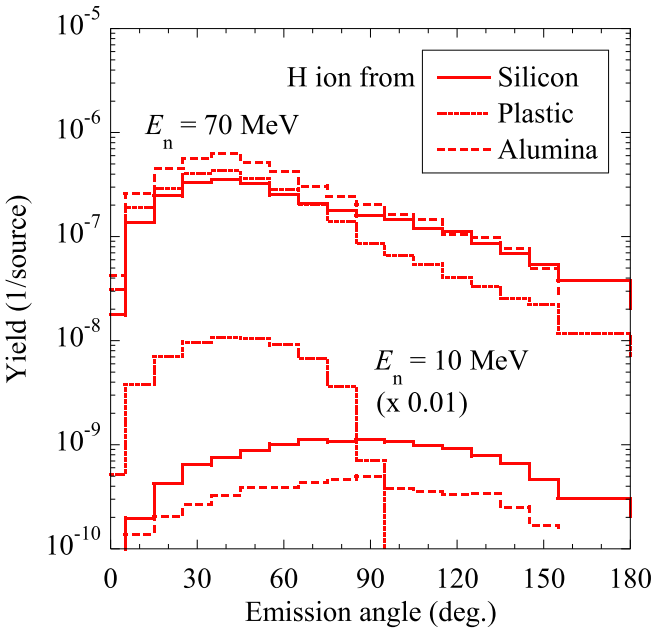

Fig. 11. Emission angle of secondary H ions from each material with the neutron energies of 10 and 70 MeV.

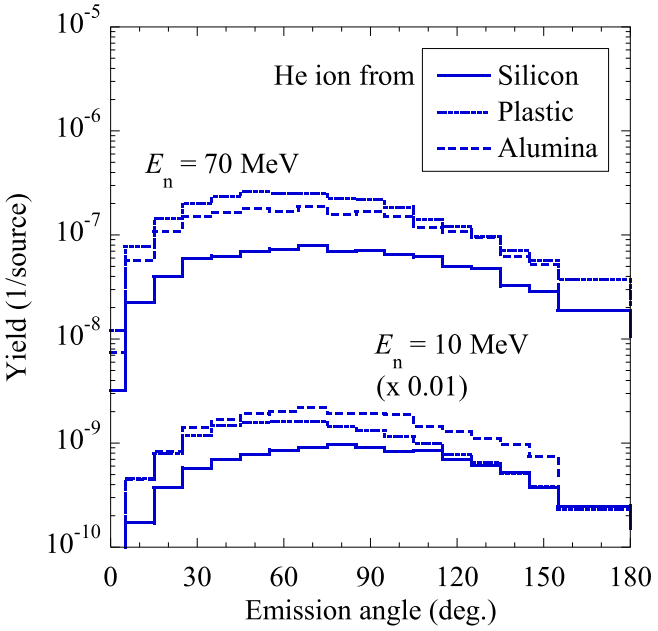

Fig. 12. Emission angle of secondary He ions from each material with the neutron energies of 10 and 70 MeV. Lines are for eye guide.

were simulated. Figs. 11–13 show the angular distributions and production yields of secondary H and He ions from each target. Secondary H and He ions generated from plastic tended to be emitted to more forward angles than those from the others. In particular, almost all of the secondary H ions from plastic with neutron energy of 10 MeV were emitted to forward angles. This is because the Q values (i.e., a negative value for the threshold energy) of the ^{12}C(n, p) and ^{16}O(n, p) reactions are −12.59 and −9.64 MeV, respectively [24]. Thus, almost all of the H ions were generated via elastic scattering with hydrogen atoms, which were only in the plastic in this simulation. The elastic scattering cross section increased

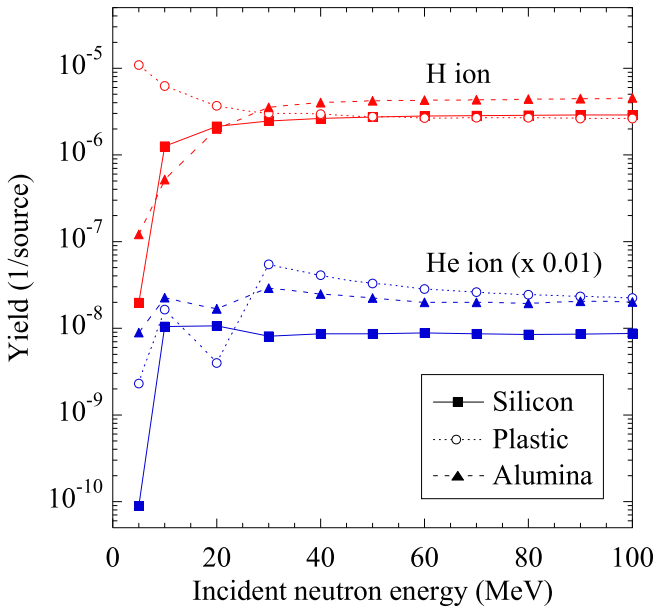

Fig. 13. Production yields of secondary H and He ions for each neutron energy.

with decreasing neutron energy below several tens of MeV, whereas that of the spallation reaction decreased as the neutron energy decreased, as shown in Fig. 13. Moreover, there was no threshold energy for elastic scattering, while the spallation reaction had a threshold energy. Thus, the contribution of H ions to the SEU cross sections for the plastic package side irradiation was larger than those for the others in the low neutron energy domain.

The amount of He ions from the plastic was three to seven times more than that from silicon except at neutron energies from 10 to 20 MeV. We also investigated the accuracy of the nuclear reaction models, and the reaction cross section of ^{12}C(n, xα) at neutron energy of 14 MeV was found to be 74 mb by PHITS, whereas that from experiments [25] was 402 ± 46 mb. This underestimation is attributed to the fact that the cross section data for ^{12}C(n, n'2α)^{4}He is not included in JENDL-4.0. It seems that this underestimation is the cause of the underestimation of the experimental result obtained via irradiation with quasi-monoenergetic neutrons with a peak energy of 23 MeV from the board side. Of note, the range of secondary ions is almost the same in plastic and silicon because the number density of electrons for plastic is almost the same as that for silicon.

V. Conclusion

A test board equipped with 65-nm bulk CMOS SRAMs was irradiated with quasi-monoenergetic neutrons from the package side and from the board side. The number of SEUs obtained by the board-side irradiation was approximately 20% to 30% less than that obtained for the package-side irradiation. SEU cross sections were estimated from the simulation of monoenergetic neutron irradiation on a test device using the PHITS and the MSV model. SEU cross sections for the plastic package-side irradiation were larger than those for the board-side and the alumina package-side irradiations because of the difference in production yield and angular distribution of H and He ions. In particular, there is a considerable difference in H ion production with low-energy neutrons, because plastic as a package contains hydrogen atoms and H ions can be generated via elastic scattering. Elastic scattering generates H ions only for forward emission; therefore, SEU cross sections increased upon plastic package-side irradiation. We calculated the SER from the SEU cross section and secondary cosmic-ray neutron flux obtained by the PARMA model. The SER obtained from the plastic package-side irradiation was approximately twice larger than that from the board-side irradiation. Thus, the material and the irradiated side of the test board should be reported when acceleration test results are published. To conclude, SERs can be reduced by equipping devices with a plastic package side that faces downward.

Acknowledgment

The authors would like to thank Prof. M. Itoh for his kind cooperation in the experiment at CYRIC, Tohoku University.

References

[1] *Measurement and Reporting of Alpha Particle and Terrestrial Cosmic Ray-Induced Soft Errors in Semiconductor Devices*, JEDEC Standard JESD89A, Oct. 2006. [Online]. Available: http://www.jedec.org

[2] S. A. Wender *et al.*, "A fission ionization detector for neutron flux measurements at a spallation source," *Nucl. Instrum. Methods Phys. Res. A, Accel. Spectrom. Detect. Assoc. Equip.*, vol. 336, nos. 1–2, pp. 226–231, 1993.

[3] E. W. Blackmore, P. E. Dodd, and M. R. Shaneyfelt, "Improved capabilities for proton and neutron irradiations at TRIUMF," in *Proc. IEEE Radiat. Effects Data Workshop*, CA, USA, Jul. 2003, pp. 149–155.

[4] Y. Iwamoto *et al.*, "Evaluation of the white neutron beam spectrum for single-event effects testing at the RCNP cyclotron facility," *Nucl. Technol.*, vol. 173, no. 2, pp. 210–217, 2011.

[5] A. V. Prokofiev, J. Blomgren, R. Nolte, S. P. Platt, S. Röttger, and A. N. Smirnov, "Characterization of the ANITA neutron source for accelerated see testing at the svedberg laboratory," in *Proc. Eur. Conf. Radiat. Effects Compon. Syst.*, Sep. 2008, pp. 260–267.

[6] S. Abe *et al.*, "Neutron-induced soft error analysis in MOSFETs from a 65 nm to a 25 nm design rule using multi-scale Monte Carlo simulation method," in *Proc. IEEE Int. Rel. Phys. Symp. (IRPS)*, 2012, pp. SE.3.1–SE.3.6.

[7] S.-I. Abe and Y. Watanabe, "Analysis of charge deposition and collection caused by low energy neutrons in a 25-nm bulk CMOS technology," *IEEE Trans. Nucl. Sci.*, vol. 61, no. 6, pp. 3519–3526, Dec. 2014.

[8] Y. Sakemi, M. Itoh, and T. Wakui, "High intensity fast neutron beam facility at CYRIC," *Int. Atomic Energy Agency*, vol. 46, no. 9, pp. 229–233, 2014.

[9] S. Hirokawa, R. Harada, K. Sakuta, Y. Watanabe, and M. Hashimoto, "Multiple sensitive volume based soft error rate estimation with machine learning," in *Proc. 16th Eur. Conf. Radiat. Effects Compon. Syst. (RADECS)*, Sep. 2016, pp. 1–4.

[10] W. Liao *et al.*, "Measurement and mechanism investigation of negative and positive muon-induced upsets in 65-nm bulk SRAMs," *IEEE Trans. Nucl. Sci.*, vol. 65, no. 8, pp. 1734–1741, Aug. 2018.

[11] T. Sato *et al.*, "Features of particle and heavy ion transport code system (PHITS) version 3.02," *J. Nucl. Sci. Technol.*, vol. 55, no. 6, pp. 684–690, 2018.

[12] T. Ogawa, T. Sato, S. Hashimoto, and K. Niita, "Development of a reaction ejectile sampling algorithm to recover kinematic correlations from inclusive cross-section data in monte-carlo particle transport simulations," *Nucl. Instrum. Methods Phys. Res. A, Accel. Spectrom. Detect. Assoc. Equip.*, vol. 763, pp. 575–590, 2015.

[13] T. Ogawa, T. Sato, S. Hashimoto, and K. Niita, "New algorithm for Monte Carlo particle-transport simulation to recover event-by-event kinematic correlations of reactions emitting charged particles," in *Proc. Joint Int. Conf. Math. Comput., Supercomput. Nucl. Appl. Monte Carlo Method*, Nashville, TN, Apr. 2015, pp. 1–11.

[14] K. Shibata *et al.*, "JENDL-4.0: A new library for nuclear science and engineering," *J. Nucl. Sci. Technol.*, vol. 48, no. 1, pp. 1–30, 2011.
[15] A. Boudard, J. Cugnon, J.-C. David, S. Leray, and D. Mancusi, "New potentialities of the Liège intranuclear cascade model for reactions induced by nucleons and light charged particles," *Phys. Rev. C, Nucl. Phys.*, vol. 87, Jan. 2013, Art. no. 014606.
[16] S. Furihata, "Statistical analysis of light fragment production from medium energy proton-induced reactions," *Nucl. Instrum. Methods Phys. Res. B, Beam Interact. Mater. At.*, vol. 171, no. 3, pp. 251–258, 2000.
[17] S.-I. Abe and T. Sato, "Soft error rate analysis based on multiple sensitive volume model using PHITS," *J. Nucl. Sci. Technol.*, vol. 53, no. 3, pp. 451–458, 2016.
[18] N. Kotani, "TCAD in Selete," in *Proc. Simulation Semiconductor Process. Devices*, 1998, pp. 3–7.
[19] T. Wada *et al.*, "ENEXSS a 3-dimensional TCAD system," (in Japanese), in *Proc. Ext. Abstr. 53rd Spring Meeting Jpn. Soc. Appl. Phys.*, 2006, p. 7.
[20] M. Nakamura, "Current status and subjects on practical 3D TCAD for next generation," (in Japanese), *Jpn. Soc. Appl. Phys.*, vol. 77, no. 7, pp. 818–822, 2008.
[21] S. Abe *et al.*, "Multi-scale Monte Carlo simulation of soft errors using PHITS-HyENEXSS code system," *IEEE Trans. Nucl. Sci.*, vol. 59, no. 4, pp. 965–970, Aug. 2012.
[22] T. Sato, "Analytical model for estimating terrestrial cosmic ray fluxes nearly anytime and anywhere in the world: Extension of PARMA/EXPACS," *PLoS ONE*, vol. 10, no. 12, 2015, Art. no. e0144679.
[23] T. Sato, "Analytical model for estimating the zenith angle dependence of terrestrial cosmic ray fluxes," *PLoS ONE*, vol. 11, no. 8, 2016, Art. no. e0160390.
[24] G. Audi and A. H. Wapstra, "The 1995 update to the atomic mass evaluation," *Nucl. Phys. A*, vol. 595, no. 4, pp. 409–480, 1995.
[25] R. C. Haight, S. M. Grimes, R. G. Johnson, and H. H. Barschal, "The ^{12}C(n,a) reaction and the kerma factor for carbon at E_n=14.1 MeV," *Nucl. Sci. Eng.*, vol. 87, no. 1, pp. 41–47, 1984.